Molecular Dynamics Simulation of *n*-Butane−Methane Mixtures in Silicalite

Leonidas N. Gergidis and Doros N. Theodorou*

Department of Chemical Engineering, University of Patras, and Institute of Chemical Engineering and High-Temperature Chemical Processes, GR 26500 Patras, Greece

Received: September 11, 1998; In Final Form: January 25, 1999

The transport of *n*-butane−methane mixtures in the zeolite silicalite has been studied. We have used long molecular dynamics simulations for the calculation of diffusion tensor components for both species over a wide range of loadings and compositions at 300 K. Self-diffusivities are seen to decrease monotonically with loading of either species. Raising the loading of *n*-butane from 2 to 9 molecules per unit cell causes the diffusivity of methane to drop by a factor of 60. The spatial distribution of molecules of the two co-adsorbed species was investigated, showing that, at high occupancies, *n*-butane molecules force methanes to partially abandon straight channel interiors and occupy the intersection regions. A conformation analysis indicates that, at high methane concentrations, *n*-butane molecules are forced to populate preferentially the gauche conformation. We have identified an anomalous diffusion regime for both species at higher loadings. Interestingly, anomalous effects are more pronounced for methane than for *n*-butane in all three directions, but most strongly in the *z*-direction, along which no direct channel pathway exists. Crossover to normal "Fickian" diffusion occurs at times on the order of nanoseconds. Visualization of trajectories from the dynamic simulations reveals a jumplike character of intracrystalline motion. We have studied the interaction energies for each species in each of the three silicalite environments. Sorbate−sorbate energy distributions show a strong concentration dependence.

1. Introduction

In recent years, molecular simulation techniques have been used widely to study sorbate molecules confined within microporous materials, such as zeolites. Such techniques constitute a powerful tool for elucidating a number of structure−property relationships and predicting sorption thermodynamics and transport rates relevant to many industrial applications. Zeolites are widely used as catalysts in the petroleum and petrochemical industry in a number of processes, such as xylene isomerization, catalytic dewaxing, and methanol conversion to gasoline. They are important in water cleaning and softening as selective adsorbents.[1,2] Zeolites are also used in industrial separations, such as pressure swing adsorption (PSA)[3] and membrane-based processes. Basic features of zeolites in these applications are high thermal/hydrothermal stability and hydrophobic/organophilic adsorptive properties. Both from a theoretical and an experimental point of view, zeolites offer excellent opportunities for understanding transport processes in porous media[4] due to their unique, well-defined crystal structure. ZSM-5, in particular, enables desirable shape selectivity. This property of zeolites is intimately related to their pore topology and diameter, the latter being comparable to molecular dimensions.

The dynamical behavior of sorbed molecules is crucial in determining the performance of zeolites in catalytic or separation processes. For example, for rapid chemical reactions, the overall rate of reaction can be affected significantly by intracrystalline diffusion resistances. The molecular dynamics (MD) technique is suitable for the elucidation of rates and mechanisms of molecular motion, which are often difficult to obtain experimentally. The dynamical properties of sorbed molecules can be described or derived from fundamental knowledge of the structure and energetics.

Using as input appropriate interaction potentials (from empirical force fields or quantum mechanical calculations) and the crystal structure, statistical mechanics-based molecular simulations have been conducted since the late 1980s for the calculation of thermodynamic properties of pure sorbates.[5,6] These properties can be compared directly with experimental data, such as sorption isotherms and isosteric heats. Additional information from the simulations includes the siting preferences of sorbate molecules.

Binary or multicomponent mixtures have not received as much attention as pure sorbates, although it is multicomponent behavior that is of most interest in practical applications. Only few, fairly recent studies exist. The majority of these studies have focused on the sorption thermodynamics. Razmus and Hall[7] have reported selectivities for N_2-O_2 mixtures in the zeolite 5A based on grand canonical Monte Carlo (GCMC) simulations. Karavias and Myers[8] have also conducted GCMC simulations for three binary systems, $C_2H_4-CO_2$, CH_4-CO_2, and i-$C_4H_{10}-C_2H_4$, in a zeolite X cavity. Phase diagrams and total coverage were calculated at room temperature in good agreement with experiment, except for the system containing i-C_4H_{10} and C_2H_4. The adsorption of an equimolar gas mixture of nitrogen and methane in zeolite Y was studied by Maddox and Rowlinson.[9] Van Tassel and co-workers[10,11] studied with GCMC the adsorption of small molecules, such as Xe, Ar, and CH_4, over a wide range of pressures. They also studied the pressure dependence of the selectivity in both Xe−Ar and Xe−CH_4 mixtures, showing very interesting adsorption characteristics. Buss, Heuchel, and Snurr[12,13] have reported results obtained by experiments, theory, and simulations for binary

* Author to whom correspondence should be addressed at the University of Patras. Phone: +3061-997-398. Fax: +3061-993-255. E-mail: doros@sequoia.chemeng.upatras.gr.

10.1021/jp983680p CCC: $18.00
Published on Web 04/13/1999

mixtures of CH_4-CF_4. They predicted the adsorption of methane and tetrafluoromethane in silicalite as a function of gas phase composition, total pressure, and temperature. Both for single components and mixtures, predictions of adsorption isotherms and isosteric heats were in good agreement with experiment at room temperature. A direct comparison with ideal adsorbed solution theory showed deviations for very high loadings. Also, preferential adsorption of methane in the sinusoidal and of tetrafluoromethane in the straight channels was reported, in agreement with the results obtained from MD simulations by Snurr and Kärger.[14] Experimental separation studies of hydrocarbon isomer vapors and of cyclic, branched, and linear hydrocarbon mixtures with silicalite membranes have been reported by Funke et al.[15−17] These investigations have shown that, for binary and ternary mixtures, *n*-octane permeates faster than either *n*-hexane or isooctane; a selectivity of 40 for *n*-octane over isooctane was obtained for a ternary mixture. While *n*-octane was always the faster permeating compound in such mixtures (the permeance of *n*-octane increasing by a factor of 16 in the presence of isooctane and *n*-hexane), it was reported that pure isooctane permeated up to 5 times faster than pure *n*-octane and pure *n*-hexane permeated faster than *n*-octane and isooctane in the pure state. These studies show that the behavior of pure components cannot always be used for the prediction of separations of mixtures, where it is not necessary that the largest molecule have the lowest permeance. *n*-Alkanes can be separated efficiently from mixtures with branched and cyclic compounds. Selectivities decrease as the temperature is increased. Mixtures of branched and cyclic molecules do not separate.

In the direction of predicting dynamical properties, such as self-diffusivities, of mixtures in zeolites, simulation studies are even scarcer. Chitra and Yashonath[18] have reported MD simulations for binary mixtures of Lennard-Jones spheres having identical masses but different diameters in the zeolite NaY. Their study showed that the larger sorbate would diffuse faster than the smaller sorbate. This is possible when the sorbate diameter approaches the diameter of the window. A direct comparison between MD simulations and experimental self-diffusivities from pulsed field gradient NMR for a binary mixture of methane−tetrafluoromethane was made by Snurr and Kärger.[14] The reported self-diffusivities from the simulations were in good agreement with the experimental measurements. These authors observed that the diffusivities for both components, at constant total loading, decreased as the fraction of the larger and less mobile CF_4 increased. Also very recently, Jost et al.[19,20] have reported MD and pulsed field gradient NMR studies for diffusion of methane−xenon mixtures over a wide range of loadings and compositions. This study showed that xenon diffusivity was unaffected by the presence of methane molecules at various concentrations. By variation of the concentration of xenon, a monotonic decrease of the diffusivity of both species was observed.

The present investigation focuses on mixtures of *n*-butane and methane in silicalite. These systems were chosen because of their practical applications and because it is methodologically and computationally feasible to conduct such an investigation. The *n*-butane molecule, a flexible alkane displaying torsion around skeletal bonds, has shown interesting behavior when confined in zeolites Y and NaCaA.[21,22] This is the first attempt to predict how this behavior is modified in the presence of coadsorbed methane and, conversely, how the siting and mobility of methane are affected by *n*-butane, which adsorbs more strongly and moves more sluggishly in the pores.

TABLE 1: Intermolecular Potential Parameters

interactions	ϵ /K	σ /Å	interactions	ϵ /K	σ /Å
CH_2,CH_3-CH_2,CH_3	72	3.923	CH_4-O	133.3	3.214
CH_2,CH_3-O	83.8	3.364	CH_2,CH_3-CH_4	103.2	3.826
CH_4-CH_4	147.95	3.73			

TABLE 2: Intramolecular Potential Parameters

k_θ/K rad^{-2}	62608	c_3/K	−368
c_0/K	1116	c_4/K	3156
c_1/K	1462	c_5/K	−3788
c_2/K	−1578		

2. Model Representation

Silicalite is the aluminum free, hence cation-free, form of the zeolite ZSM-5. As in previous simulation works, the orthorhombic form having *Pnma* symmetry is used, with lattice parameters of 20.07, 19.92, and 13.42 Å. Crystal atom positions were taken from X-ray diffraction data.[23] The lattice was taken as rigid to reduce computational requirements. The rigidity of the lattice appears to be acceptable for sorbates that do not fit tightly in the pores of the zeolite.[24−28] In silicalite there are two types of channels. One (straight) is parallel to the *y*-direction, and the other (sinusoidal or zigzag) is undulating with mean direction parallel to the *x*-direction. Motion along the *z*-direction is possible only following a tortuous path consisting of steps taken along the two channel systems. Straight and sinusoidal channels have elliptical cross sections with principal axes roughly 5.4 Å × 5.6 Å and 5.1 Å × 5.5 Å, respectively.

The *n*-butane molecules are represented in terms of four united atom methyl and methylene groups (interaction sites). Following June et al.,[29] we have used the same potential parameters for both methyl and methylene, although we have assigned the correct masses, 15 and 14 g/mol, respectively, to the two groups. Methane was modeled as a spherical molecule (single interaction site), following Goodbody et al.[25] and Maginn et al.[30] For the intermolecular interactions between sites on the sorbates (*n*-butane−*n*-butane, methane−methane, *n*-butane−methane) and for the interaction between sorbates and oxygens of the silicalite crystal, a Lennard-Jones potential was used with a cutoff distance of 13 Å:

$$V_{LJ}(r_{ij}) = 4\epsilon\left[\left(\frac{\sigma_{ij}}{r_{ij}}\right)^{12} - \left(\frac{\sigma_{ij}}{r_{ij}}\right)^{6}\right] \quad (1)$$

For *n*-butane, bond lengths were assumed rigid and constrained to a length of 1.53 Å. Bond angles and torsion angles were allowed to fluctuate under the influence of the following potentials:

$$V_{\text{bending}}(\theta) = {}^1/_2 k_\theta(\theta - \theta_{eq})^2 \quad (2)$$

$$V_{\text{torsion}}(\phi) = \sum_{k=0}^{5} c_k \cos^k(\phi) \quad (3)$$

The equilibrium value for the bond angle was $\theta_{eq} = 112°$. Values of ϵ_{ij}, σ_{ij}, k_θ, and c_k were identical to those used in refs 29 and 30 and are reproduced in Tables 1 and 2. In the pure sorbate cases, these representations have been shown to give predictions for sorption thermodynamics and diffusivity in good agreement with experiment. Cross interaction potential parameters were obtained through the Lorentz−Berthelot relations

$$\sigma_{ij} = (\sigma_{ii} + \sigma_{jj})/2 \quad (4)$$

$$\epsilon_{ij} = (\epsilon_{ii}\epsilon_{jj})^{1/2} \quad (5)$$

To improve the speed of the simulations, two pretabulated lattice-sorbate potential maps were used, for the methane−zeolite and methyl/methylene−zeolite interactions.[31]

3. Molecular Dynamics

Simulations were conducted in the microcanonical statistical ensemble (NVE) and also in the canonical ensemble (NVT) using the Nosé−Hoover thermostat.[32] Two sets of simulations were performed. In the first, the loading of *n*-butane ranged from 0 to 9 molecules/unit cell (uc) keeping the methane at 4 molecules/uc. In the second, the loading of methane ranged from 0 to 14 molecules/uc, keeping the *n*-butane at 4 molecules/uc. All results obtained from the two statistical ensembles at the same thermodynamic state points were identical, within simulation error. Thus, only results from NVE simulations are reported here. Constraint forces arising from the fixed bond lengths of *n*-butane were computed, as in previous simulation studies,[29] by the algorithm of Edberg, Evans, and Morriss.[33] Newton's equations of motion were integrated with a fifth-order predictor−corrector algorithm using a 2 fs time step,[34] which proved adequate for energy conservation, since the energy drift was lower than 0.5% over the duration of the production runs.

Initial low-energy configurations were generated using a Monte Carlo insertion and subsequent relaxation process for each species. After the equilibration period, which ranged from 0.5 ns (for small) to 2 ns (for higher occupancies), production runs were conducted for a total duration ranging from 6 ns up to 20 ns for the high occupancies. To observe the true diffusive behavior of the sorbate molecules and to calculate reliable diffusion constants it is necessary to conduct simulations of such length (see Results). This has been pointed out by Chitra and Yashonath in simulations of similar systems.[35] Of course, it should be noted that MD simulations performed on currently available computing resources are extremely inefficient as a means of estimating diffusivities below 10^{-6} cm^2/s. This statement is based on the argument that sorbate molecules, on average, must traverse a distance of about 1 unit cell (average lattice constant 17.8 Å) for a reliable self-diffusivity value to be obtainable from the simulation. For a molecule with a diffusivity of 1×10^{-6} cm^2/s, about 5.3 ns is required for this; for the lowest orientationally averaged value of the diffusivity predicted here, 7×10^{-7} cm^2/s, 7.5 ns is required. For the estimation of individual components of the self-diffusivity along different axes, the computer time requirements are even more stringent. The simulation must exceed 20 ns for diffusivity values of 1×10^{-6} cm^2/s in the *y*-direction and 90 ns for diffusivity values on the order of 1×10^{-7} cm^2/s in the *z*-direction to be obtained. In our simulations these requirements are fulfilled, except for the *n*-butane at concentrations of 8 and 9 molecules per unit cell in the *z*-direction.

Production runs were carried out on SGI Origin 200 and IBM PowerPC workstations.

4. Results

4.1. Siting of Sorbate Molecules. Past simulation studies of pure methane and pure *n*-butane in silicalite[29,31] have shown that both molecules prefer to reside in the interiors of straight (S) and sinusoidal (Z) channel segments and to avoid the more spacious channel intersection regions (I), where attractive interactions due to dispersion forces with the surrounding zeolite framework are less favorable. At high occupancies, a competition between methane and *n*-butane for their preferred Z and S environments is expected; it is interesting, therefore, to study the equilibrium structure of the mixed sorbate fluid.

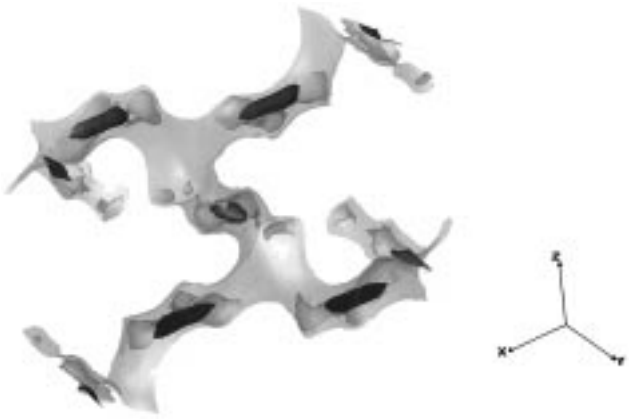

Figure 1. Center of mass distributions for *n*-butane and methane coadsorbed in silicalite at a loading of 4 molecules per unit cell of each species. The distributions are shown over half a unit cell, the other half being symmetric with respect to the *zx*-plane, i.e. the plane normal to the straight channels and containing the sinusoidal channels. Dark gray (light gray) regions enclose the spaces where the centers of mass of *n*-butane (methane) molecules spend 50% of their time with highest probability. The interior walls of the zeolite pores have been outlined in very light gray, for reference.

There are four S, four Z, and four I environments in each unit cell of silicalite. Figure 1 depicts isosurfaces of the density distribution of the centers of mass of the two sorbates inside half a unit cell, at an occupancy of 4 molecules per unit cell of methane coadsorbed with 4 molecules per unit cell of *n*-butane. The center of mass density distribution of species k ($k = 1$ for methane, $k = 2$ for *n*-butane) is defined as

$$\rho_k^1(\mathbf{r}) = \frac{1}{N_k}\{\int \sum_{i=1}^{N_k} \delta(\mathbf{r} - \mathbf{f}_{cm}(\mathbf{r}_i^{(k)})) \exp[-\beta V(\mathbf{r}_1^{(1)}, ..., \mathbf{r}_{N_1}^{(1)}, \mathbf{r}_1^{(2)}, ..., \mathbf{r}_{N_2}^{(2)})] \, d^3r_1^{(1)} ... d^3r_{N_1}^{(1)} \, d^9r_1^{(2)} ... d^9r_{N_2}^{(2)}\} / \{\int \exp[-\beta V(\mathbf{r}_1^{(1)}, ..., \mathbf{r}_{N_1}^{(1)}, \mathbf{r}_1^{(2)}, ..., \mathbf{r}_{N_2}^{(2)})] \, d^3r_1^{(1)} ... d^3r_{N_1}^{(1)} \, d^9r_1^{(2)} ... d^9r_{N_2}^{(2)}\} \quad (6)$$

with $\mathbf{r}_i^{(k)}$ being the vector of generalized coordinates describing the configuration of molecule i of species k, $d^3r_i^{(1)}$ and $d^9r_i^{(2)}$ being differential volume elements in the configuration space of one molecule, including the Jacobian of transformation from Cartesian to generalized coordinates in the case of *n*-butane.[31,36] V is the total potential energy function, and $\mathbf{f}_{cm}(\mathbf{r}_i^{(k)})$ is a vector function giving the center of mass position of molecule i of species k. Clearly, $\mathbf{f}_{cm}(\mathbf{r}_i^{(1)}) = \mathbf{r}_i^{(1)}$ in the case of methane. In practice, the densities $\rho_k^1(\mathbf{r})$ are computed by binning, throughout the production phase of the simulation, all molecular centers of mass in a three-dimensional grid with interval length 0.2 Å running through the asymmetric unit of the unit cell. The isosurfaces in all figures shown here have been constructed so that they enclose 50% of the molecular centers of mass of each component; i.e., they display the surfaces $\rho_k^1(\mathbf{r}) = \rho_k^*$, with $\int \rho_k^1(\mathbf{r}) H[\rho_k^1(\mathbf{r}) - \rho_k^*] \, d^3r = 1/2$, H being the Heaviside function.

At an occupancy of 4 molecules per unit cell of each species, the siting distributions revealed by Figure 1 are very similar to those obtained for the pure species at low occupancy.[31] Both methane and *n*-butane prefer the interiors of straight and sinusoidal channel segments and avoid channel intersections. The distribution of methane is more delocalized.

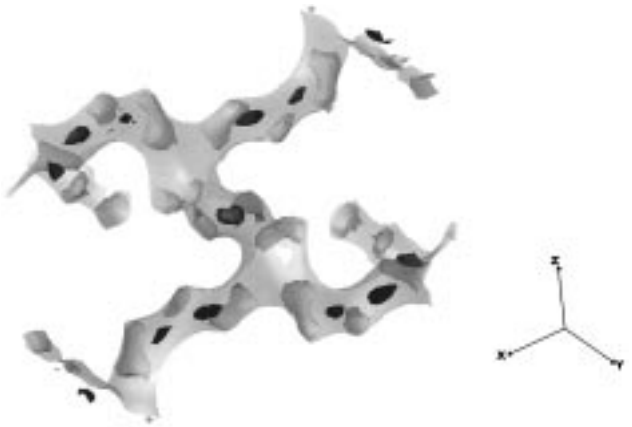

Figure 2. Same as Figure 1, but at an occupancy of 14 molecules per unit cell methane and 4 molecules per unit cell *n*-butane.

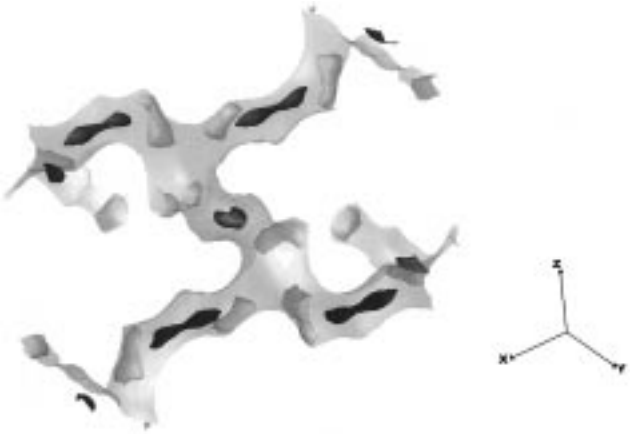

Figure 3. Same as Figure 1, but at an occupancy of 4 molecules per unit cell methane and 9 molecules per unit cell *n*-butane.

The corresponding distributions of the two species for the same occupancy of *n*-butane but a much higher occupancy of methane (14 molecules per unit cell) is shown in Figure 2. One can see significant changes in the distribution of the model fluid, induced by sorbate−sorbate interactions in the confined space of the pores. The structure is sharper, consisting of nonoverlapping, well-defined regions throughout the pore interiors. Within each sinusoidal channel segment, the cloud of *n*-butane centers of mass has now broken up into two lobes, indicating two modes of siting in these channels. Butane is still localized in the interiors of straight and sinusoidal channels, where its four skeletal segments can best take advantage of attractive interactions with the zeolite framework. Methane, however, is partly pushed out into the channel intersections. Methane's greater tendency to redistribute itself with changing occupancy can be viewed as resulting from a balance between adsorption energy and translational entropy. Displacing a *n*-butane molecule from an energetically favorable region of the zeolite entails an energetic cost comparable to that of displacing 3 or 4 methanes from the same region, while the entropy gain from delocalizing the methane molecules is much greater. At the occupancy of Figure 2, this redistribution can occur while keeping the least energetically favorable central region of the intersections free of molecular centers of mass.

Figure 3 displays the center of mass distributions in a mixed sorbate fluid consisting of 4 molecules per unit cell of methane and 9 molecules per unit cell of *n*-butane. Comparing with Figure 1, one again sees that the loci of molecular centers of mass have been reduced to well-separated, well-defined regions.

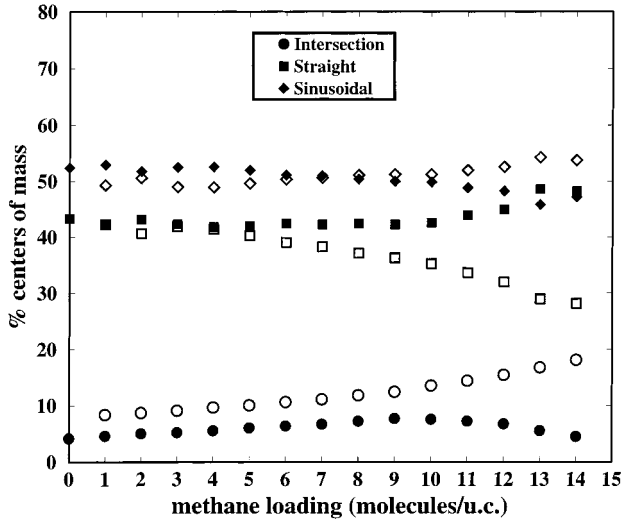

Figure 4. Percentage of centers of mass of sorbed *n*-butane (filled symbols) and methane (open symbols) molecules lying in each of the three environments of the zeolite intracrystalline space (straight channels, squares; sinusoidal channels, diamonds; intersections, circles) at various occupancies. The *n*-butane loading is kept constant at 4 molecules per unit cell, while that of methane is varied from 0 to 14 molecules per unit cell.

Butane still prefers the channel interiors; its spatial distribution within each channel segment is not quite bimodal, as in the case of Figure 2, but has developed a "waist" in the middle. Methanes are again pushed out toward the intersection regions. An important difference of Figure 3 from Figure 2 is the absence of methane clouds from the middle regions of channel segments. Under the occupancy conditions of Figure 3, practically all channel segments of the zeolite contain at least one *n*-butane molecule. Methane molecules have to share the channel segments with these *n*-butanes; they can sit near either end of a *n*-butane but are excluded from the middle regions.

Using the techniques described in refs 31, 24, 29, and 36 we have partitioned the intracrystalline space of the zeolite into S, Z, and I regions by identifying minima, saddle points, and dividing surfaces of the methane−zeolite potential. This allows us to quantify the percentage of molecules of each species which find themselves in each one of the three environments, as a function of occupancy. Results are shown in Figures 4 and 5. In Figure 4, the *n*-butane loading is held constant at 4 molecules per unit cell, while the methane loading is varied from 1 to 14 molecules per unit cell. In Figure 5 the methane loading is kept constant at 4 molecules per unit cell and that of *n*-butane is varied between 1 and 9 molecules per unit cell. From both figures we see that, at low occupancies, the distribution of the two sorbates among the S, Z, and I environments is very similar. The majority of the sorbed molecules is divided almost equally between straight and sinusoidal channels, the latter being somewhat more favorable for both species; the percentage of molecules finding themselves in intersection regions is ca. 5% for n-butane and higher (ca. 8%) for methane, which is expected to be more delocalized for the reasons discussed above. As the methane loading increases at constant *n*-butane loading (Figure 4), *n*-butane continues to localize in the channel interiors, the difference between *n*-butane populations residing in the straight and in the sinusoidal channels becoming smaller and smaller. The *n*-butane population in the intersections varies only little, exhibiting a shallow maximum around 9 methane molecules per unit cell. On the contrary, the siting preferences of methane change significantly with loading in Figure 4. While the percentage of methane molecules in sinusoidal channels remains

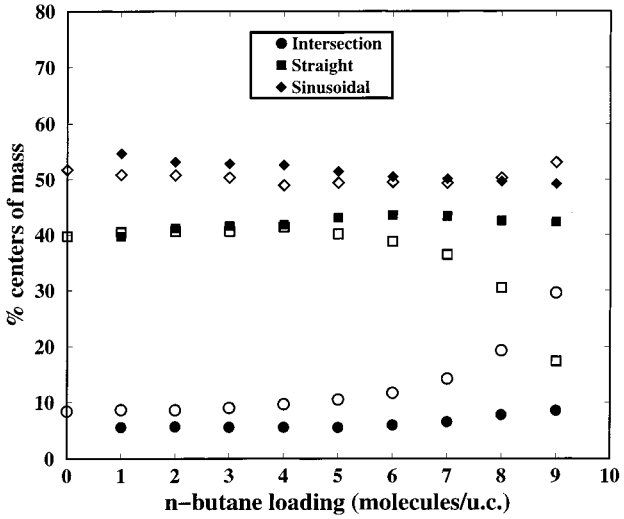

Figure 5. As in Figure 4, but with the methane loading held constant at 4 molecules per unit cell and the *n*-butane loading being varied from 0 to 9 molecules per unit cell.

largely unaffected, there is a gradual shift of methane population from straight channels into intersection regions as more and more methane is placed in the system. This confirms the observation, made in relation to Figure 2, that methane is pushed out into the intersections; furthermore, it clarifies that this happens at the expense of methane populating the straight channels, in which *n*-butane tends to concentrate preferentially at high loadings.

The population changes seen in Figure 5, as *n*-butane loading is increased at constant methane loading, are similar but more dramatic than in the case of Figure 4. Butane preferences change very little as more and more *n*-butane is added to the system. On the contrary, the siting of methane shifts rapidly with increasing loading beyond 6 *n*-butane molecules per unit cell, leading to an inversion in the relative magnitudes of S and I populations of methane at 9 *n*-butane molecules per unit cell. At this occupancy, 30% of the methane molecules find themselves in intersection regions, where the ratio of methane to *n*-butane molecules is enriched by more than a factor of 3 relative to the ratio of overall concentrations of these molecules in the zeolite.

The picture of structure of the mixed sorbed fluid is completed by the pair distribution functions $g(r)$ of molecular centers of mass, shown in Figures 6 and 7 for occupancy levels of 4 methane and 4 *n*-butane molecules per unit cell and 4 methane and 9 *n*-butane molecules per unit cell, respectively.

At low occupancy of both components (Figure 6), the most significant feature of $g(r)$ is the first peak, indicating the most probable distance between sorbate molecules sitting next to each other in the channels and held together by dispersive forces. The sharp peaks at 12−13 Å are induced by the periodicity of the zeolite field; they are due to sorbate molecules residing in different straight channel segments or different sinusoidal channel segments and are obtained even when sorbate−sorbate interactions are turned off.[37] First peaks in the methane−methane and *n*-butane−methane pair distribution function appear at approximately 4 and 5.5 Å, respectively; these would be expected for a methane van der Waals diameter of approximately 4 Å and an *n*-butane van der Waals length of approximately 7 Å in the trans conformation. With increasing occupancy (Figure 7) these first peaks shift to somewhat shorter distances and become much more pronounced. Particularly striking is the height of the methane−methane peak in Figure 7, indicating

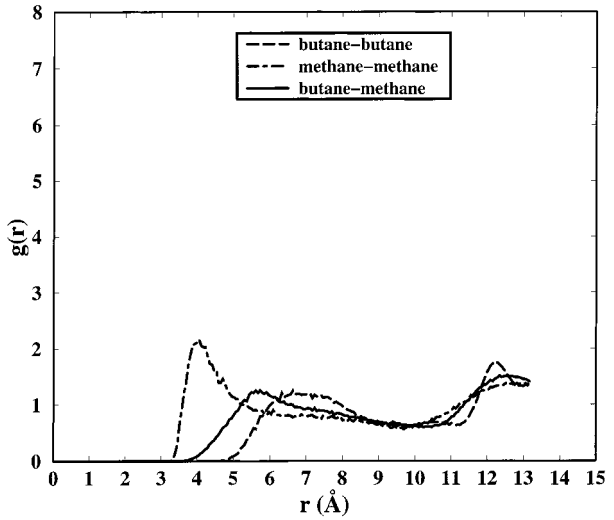

Figure 6. Pair distribution functions for the centers of mass of sorbate molecules: methane−methane (dot−dashed line); *n*-butane−*n*-butane (dashed line); and *n*-butane−methane (solid line). Loading: 4 methane molecules per unit cell and 4 *n*-butane molecules per unit cell.

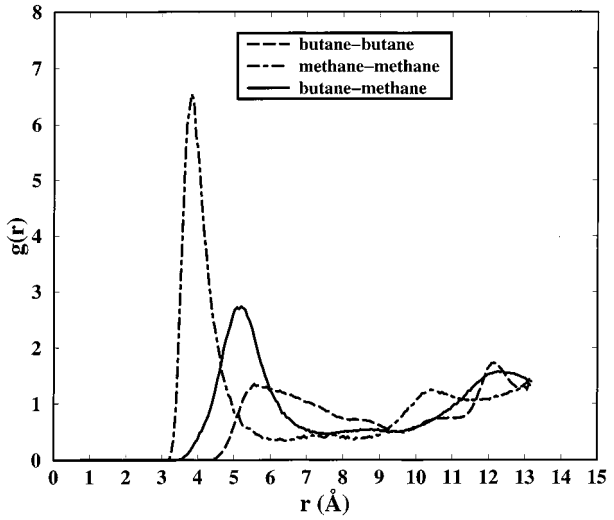

Figure 7. As in Figure 6, but for a loading of 4 methane molecules per unit cell and 9 *n*-butane molecules per unit cell.

that the few methanes present in the system tend to sit in pairs on the same side of a *n*-butane molecule. Of the pairs of molecules contributing to this very sharp peak, 39.8% reside in adjacent sinusoidal and intersection regions, 30.2% reside exclusively in sinusoidal channel segments, 6.5% reside in adjacent sinusoidal and straight channel segments, 13.2% in adjacent straight and intersection regions, and 10.3% exclusively in straight channel interiors.

The broad peak (6.5−7.5 Å) in the *n*-butane−*n*-butane $g(r)$ seen in Figure 6 contains contribution mainly (75%) from *n*-butane molecules located in adjacent straight and sinusoidal channel segments. In the system with 4 methane and 9 *n*-butane molecules per unit cell (Figure 7), the dominant *n*-butane−*n*-butane peak is slightly above 5.5 Å, indicating a significant population of compact *n*-butane pairs sitting next to each other. Contributions to this peak are 46.2% from pairs located in adjacent straight and sinusoidal channel interiors, 17.8% and 17% from molecules in sinusoidal−intersection and straight−intersection regions, respectively, 13.8% from *n*-butanes in adjacent sinusoidal channels, and 5.2% from neighboring molecules sitting in straight channels.

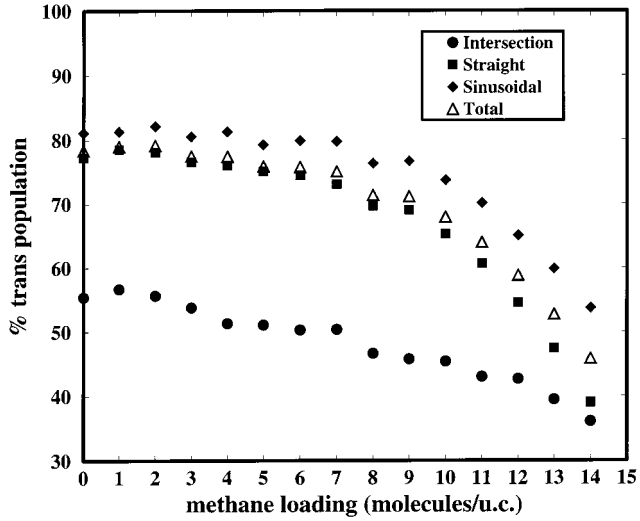

Figure 8. Percent trans population of sorbed *n*-butane in the three different intracrystalline environments of silicalite as a function of the methane loading. The *n*-butane loading is held constant at 4 molecules per unit cell.

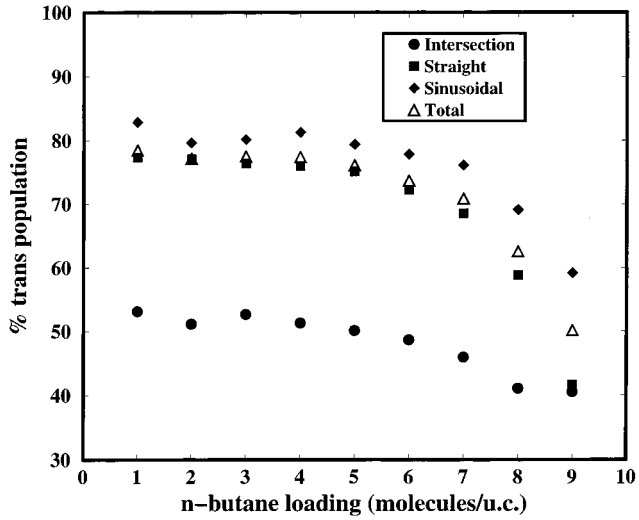

Figure 9. Percent trans population of sorbed *n*-butane in the three different intracrystalline environments of silicalite as a function of the *n*-butane loading. The methane loading is kept constant at 4 molecules per unit cell.

4.2. Conformation of *n*-Butane. It is interesting to track the conformational distribution of the flexible sorbate (*n*-butane) as a function of the occupancy and composition of the sorbate phase. The simulation trajectory can be analyzed straightforwardly to categorize *n*-butane molecules present in each configuration into the trans, gauche$^+$, and gauche$^-$ conformational states.[29] The average populations of the latter two states are equal to an excellent approximation in all cases studied here, indicating that the simulations are well-equilibrated conformationally. Figure 8 displays the % trans population as a function of the methane loading for a system containing 4 molecules of *n*-butane per unit cell. Corresponding results for the % trans population of *n*-butane as a function of the *n*-butane loading for a system containing 4 molecules of methane per unit cell are displayed in Figure 9. The statistical error in the data presented in these figures is 1−2%. At low occupancy, the population distribution in both figures is within the error bars of the distribution reported in ref 29 for a pure sorbate phase of 4 *n*-butane molecules per unit cell at 300 K. Relative to the liquid phase (approximately 61% trans population for the torsional potential employed here), trans states are strongly enhanced in the sinusoidal and straight channels and somewhat suppressed in the channel intersections.

Increasing the methane loading at constant loading of 4 molecules of *n*-butane per unit cell (Figure 8) affects the conformational distribution in the channels only little up to 7 methane molecules per unit cell. For higher methane loadings there is a significant reduction in % trans in the sinusoidal and, especially, in the straight channels, which becomes dramatic beyond 10 methane molecules per unit cell. The physical reason for this is clear; *n*-butane molecules are driven toward a more compact shape, which allows a larger number of sorbate molecules to be packed in the channel segments and benefit from the more favorable attractive interactions with the zeolite encountered there. At 14 methane molecules per unit cell, less than 40% of the *n*-butanes sorbed in straight channels (which are the most probable site for *n*-butanes at this occupancy; compare Figure 4) find themselves in the trans conformational state. The conformational distribution of the few *n*-butanes residing in channel intersections shows a much more gradual shift toward gauche throughout the range of methane loadings studied.

Increasing the *n*-butane loading at constant loading of 4 molecules of methane per unit cell (Figure 9) has similar consequences on *n*-butane conformation. The conformational distribution in the channels is affected little up to 6 molecules of *n*-butane per unit cell but shifts rapidly toward gauche beyond that occupancy. At 9 molecules of *n*-butane per unit cell, the trans population in straight channels is almost equal to that in the intersections. The very sharp drop in trans population in the straight channels indicates that, when the *n*-butane molecules sorbed are more than the channel segments in the zeolite, excess molecules localize preferentially in the straight channels. We note that similar enhancement of the gauche conformational state with increasing occupancy has been observed in simulations of *n*-butane sorbed in zeolites Y and NaCaA.[21,22]

4.3. Anomalous Diffusion. A major objective of this work has been to quantify how the self-diffusivities of methane and *n*-butane in the mixed sorbate phase depend on the loadings of the two species. For each of the MD runs conducted, the center of mass mean-squared displacement $\langle (r_\alpha^{(k)}(t) - r_\alpha^{(k)}(0))^2 \rangle$ was tracked for each species k ($k = 1, 2$) along each coordinate direction α ($\alpha = x, y, z$) as a function of time t. The angular brackets denote averaging over all molecules of species k and over different time origins along the recorded equilibrium trajectory.

Plots of $\langle (r_\alpha^{(k)}(t) - r_\alpha^{(k)}(0))^2 \rangle$ against time t, as obtained from a system containing 4 molecules of methane and 8 molecules of *n*-butane per unit cell at 300 K, are shown in Figures 10 and 11 in log−log coordinates. A first striking observation on these plots is that there is a pronounced "anomalous diffusion" regime, over which $\langle (r_\alpha^{(k)}(t) - r_\alpha^{(k)}(0))^2 \rangle \propto t^n$ with $n < 1$. The anomalous regime is shortest for motion in the y direction of the straight channels, along which translational diffusion is fastest for either species,[29,38] and longest in the z-direction of slowest motion, along which translation occurs through a combination of displacements along straight and sinusoidal channel segments. In the z-direction, crossover to normal ("Fickian") diffusion of methane occurs at times on the order of 5 ns; for *n*-butane, the anomalous regime is even more extended.

Anomalous diffusion is caused by fast, correlated motion within specific environments of the zeolite. Only after several such environments are traversed is the motion homogenized enough to appear as normal diffusion. Butane molecules display

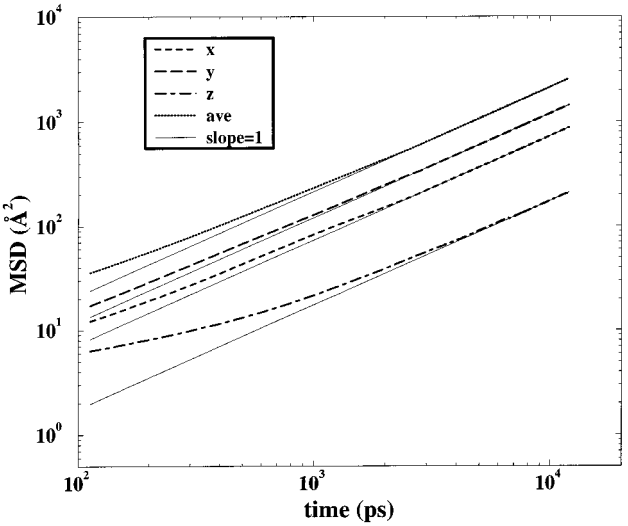

Figure 10. Mean−square displacement of methane molecules along the three coordinate directions as a function of time, in log−log coordinates. The loading is 4 molecules of methane per unit cell and 8 molecules of *n*-butane per unit cell. The thin straight lines are drawn with a slope of 1, corresponding to normal Fickian diffusion.

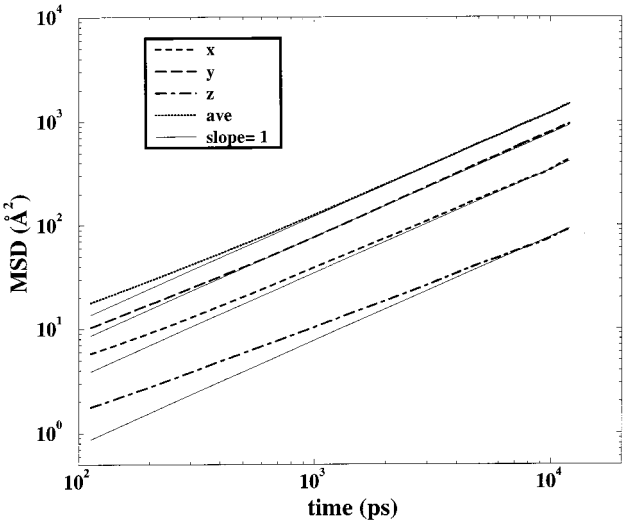

Figure 11. As in Figure 10, but for the mean−square displacement of *n*-butane centers of mass.

a strong preference for channel interiors (compare Figure 3). Translational motion is relatively facile along the axes of the channel segments but jumps between different channel interiors are required for the motion to become really diffusive. From the orientationally averaged mean-square displacement curves in Figures 10 and 11 we see that crossover to normal diffusion occurs when the root-mean-square displacement of the center of mass is approximately 18 Å, i.e. commensurate with the lattice parameters of the unit cell. Likewise, motion along the individual *x*-, *y*-, and *z*-axes becomes diffusive only when the mean-square displacement is commensurate with the unit cell size in the directions indicated.

Interestingly, the departure of the exponent *n* from unity is more pronounced for methane than for *n*-butane. One can speculate that the blocking effect exerted by the sluggish *n*-butane molecules on the fast-moving methane is more severe than the inverse effect of methane on *n*-butane motion. Molecules of *n*-butane, acting as effective blockings, induce a large amount of dynamic heterogeneity in methane motion. In the *z*-direction the exponent *n* for methane at short times

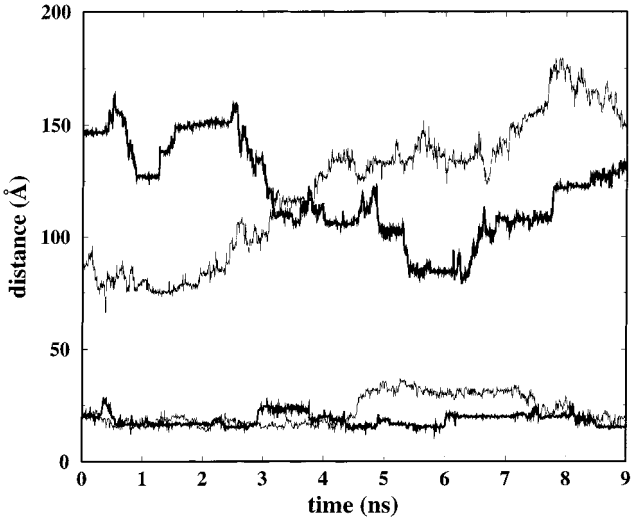

Figure 12. Distances traversed by a *n*-butane (thick lines) and a methane (thin lines) molecule, shown as functions of time for two different sorbate loadings. The upper curves are for a loading of 4 *n*-butane and 8 methane molecules per unit cell; the lower ones are for 8 *n*-butane and 4 methane molecules per unit cell. Origins for the measurement of distance are arbitrary.

becomes close to $^1/_2$, i.e. close to the value corresponding to single-file diffusion.[39]

In view of the anomalous diffusion effects, it becomes clear that MD simulations of duration exceeding several nanoseconds are necessary for a reliable estimation of the diffusivity, even in the simple methane, *n*-butane/silicalite system (compare discussion in section 3 and ref 35). We note that anomalous diffusion effects have been observed in simulations of small penetrant motion through amorphous polymers.[40] In that case, anomalous diffusion was attributable to facile, correlated motion of the penetrant along elongated cavities or strings of cavities parallel to the chains. The existence of well-defined pores in the zeolite case makes the phenomenon more pronounced (smaller *n* at short times) and more clear-cut.

4.4. Jumplike Nature of Intracrystalline Motion. Another interesting observation has to do with the jumplike character of diffusion. By the plotting of trajectories from the dynamics simulations, it is clear that molecular displacements are a combination of short oscillatory motions and of infrequent, abrupt jumplike processes taking place within short time periods (see Figure 12). It is apparent from the trajectories that molecules are trapped for periods of time. Jump lengths between successive positions vary when the concentration and composition of the mixture change. Of course, over the time scales of a few decades of nanoseconds accessed by the MD simulations we can discuss only some qualitative characteristics of these processes. From Figure 12 it is evident that, when the loading is increased, the mean jump length is reduced significantly. Intersection interiors are the natural energy barriers to molecular motion imposed from the crystal structure. By an increase of the loading, extra energy barriers arise due to the neighboring molecules, which cannot be circumvented. Large jumps performed by neighboring molecules must be highly correlated. This jump picture is intimately related to the anomalous diffusion behavior discussed above and to its dependence on loading.

4.5. Occupancy Dependence of the Self-Diffusivities. The diagonal elements of the self-diffusivity tensor, $D_{s,\alpha\alpha}^{(k)}$, for each species were extracted from the long-time, linear (Fickian) part of mean-squared displacement versus time plots (compare

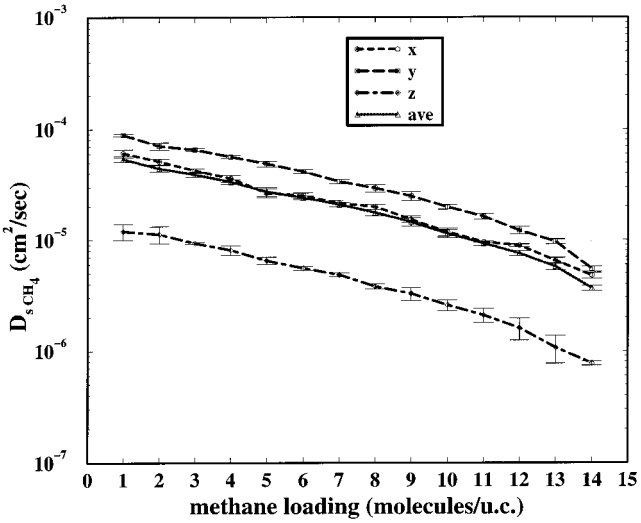

Figure 13. Elements of the self-diffusivity tensor along the *x*, *y*, and *z* directions and orientationally averaged self-diffusivity of methane in mixtures of methane and *n*-butane sorbed in silicalite at 300 K, shown as functions of the methane loading. The *n*-butane loading is held constant at 4 molecules per unit cell.

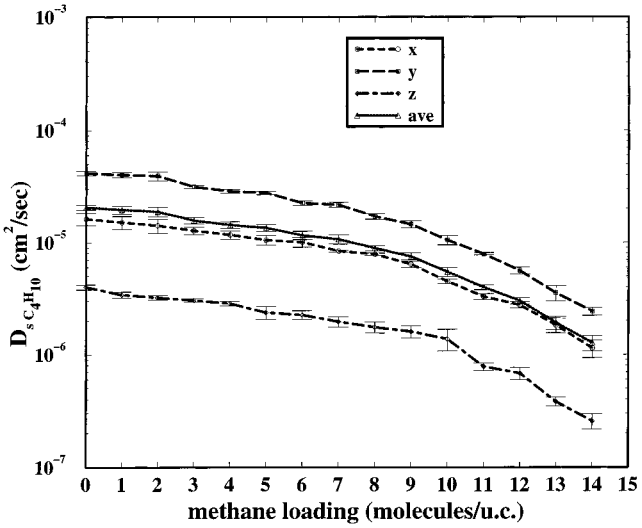

Figure 14. Elements of the self-diffusivity tensor along the *x*, *y*, and *z* directions and orientationally averaged self-diffusivity of *n*-butane in mixtures of methane and *n*-butane sorbed in silicalite at 300 K, shown as functions of the methane loading. The *n*-butane loading is held constant at 4 molecules per unit cell.

Figures 10 and 11):

$$D_{s,\alpha\alpha}^{(k)} = \frac{1}{2}\lim_{t\to\infty}\frac{d}{dt}\langle (r_\alpha^{(k)}(t) - r_\alpha^{(k)}(0))^2\rangle \qquad (7)$$

The orientationally averaged self-diffusivity, $D_s^{(k)}$, for each component was also computed as one-third the trace of the diffusivity tensor of the component. Error bars for the self-diffusivities were obtained by averaging the values extracted from the Fickian regimes of several runs carried out under the same temperature and occupancy conditions but initiated at different MC-generated configurations.

$D_{s,xx}$, $D_{s,yy}$, $D_{s,zz}$, and D_s of methane and *n*-butane in systems containing 4 *n*-butane molecules per unit cell are shown as functions of the methane loading in Figures 13 and 14, respectively. The same self-diffusivities in systems containing 4 methane molecules per unit cell are shown as functions of the *n*-butane loading in Figures 15 and 16. Semilogarithmic

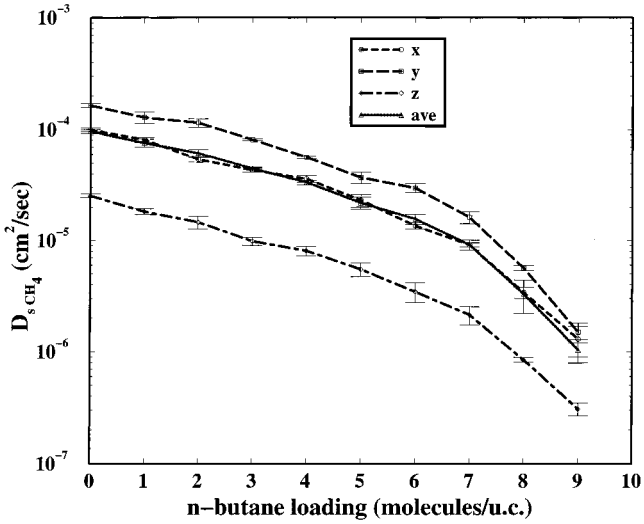

Figure 15. Elements of the self-diffusivity tensor along the *x*, *y*, and *z* directions and orientationally averaged self-diffusivity of methane in mixtures of methane and *n*-butane sorbed in silicalite at 300 K, shown as functions of the *n*-butane loading. The methane loading is held constant at 4 molecules per unit cell.

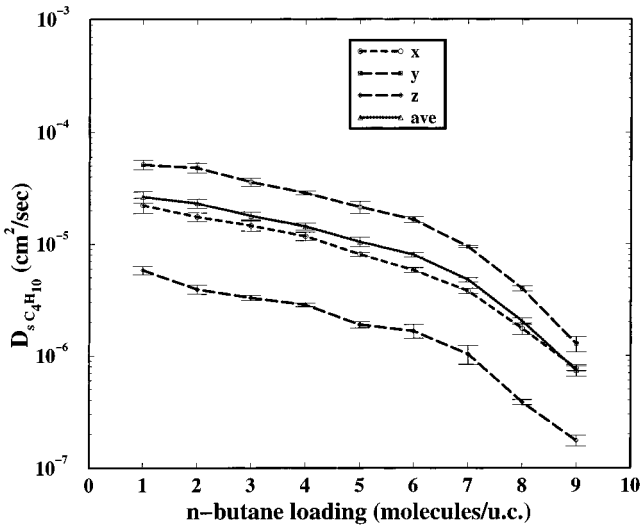

Figure 16. Elements of the self-diffusivity tensor along the *x*, *y*, and *z* directions and orientationally averaged self-diffusivity of *n*-butane in mixtures of methane and *n*-butane sorbed in silicalite at 300 K, shown as functions of the *n*-butane loading. The methane loading is held constant at 4 molecules per unit cell.

coordinates have been used to make the form of the occupancy dependence more apparent.

The diffusivity components follow the well-known relation[29,2] $D_{s,yy} > D_{s,xx} \gg D_{s,zz}$. They are decreasing functions of occupancy in all cases.

The decay of methane and *n*-butane self-diffusivities with methane occupancy (Figures 13 and 14) is rather smooth and somewhat stronger than exponential. For both species, the self-diffusivities decrease by somewhat less than 1 order of magnitude as methane loading rises from 2 to 14 molecules per unit cell at 4 *n*-butane molecules per unit cell.

The drop in methane and *n*-butane self-diffusivities with *n*-butane loading (Figures 15 and 16) can be viewed as consisting of two quasiexponential parts. The drop is gradual up to 6 *n*-butane molecules per unit cell but accelerates significantly beyond 7 *n*-butane molecules per unit cell. This is because, at these high *n*-butane occupancies, most channel interiors are occupied by a *n*-butane molecule, which acts as

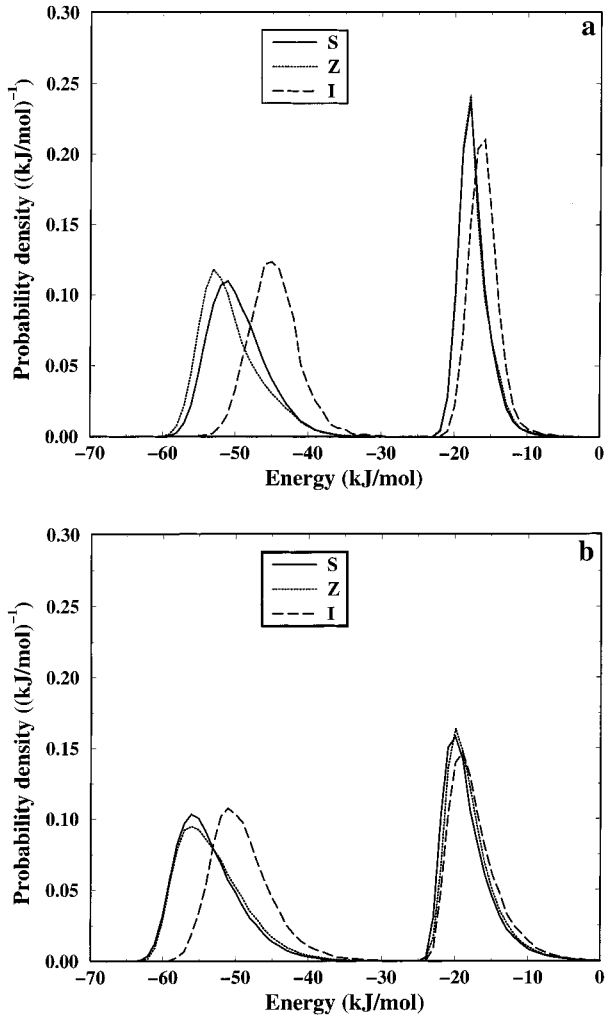

Figure 17. Energy distributions (a) at an occupancy of 4 methane and 4 *n*-butane molecules per unit cell and (b) at 4 methane and 9 *n*-butane molecules per unit cell. The total energy felt by a molecule due to the zeolite field and due to its interactions with other molecules is considered. Distributions for *n*-butane are on the left, and those for methane on the right.

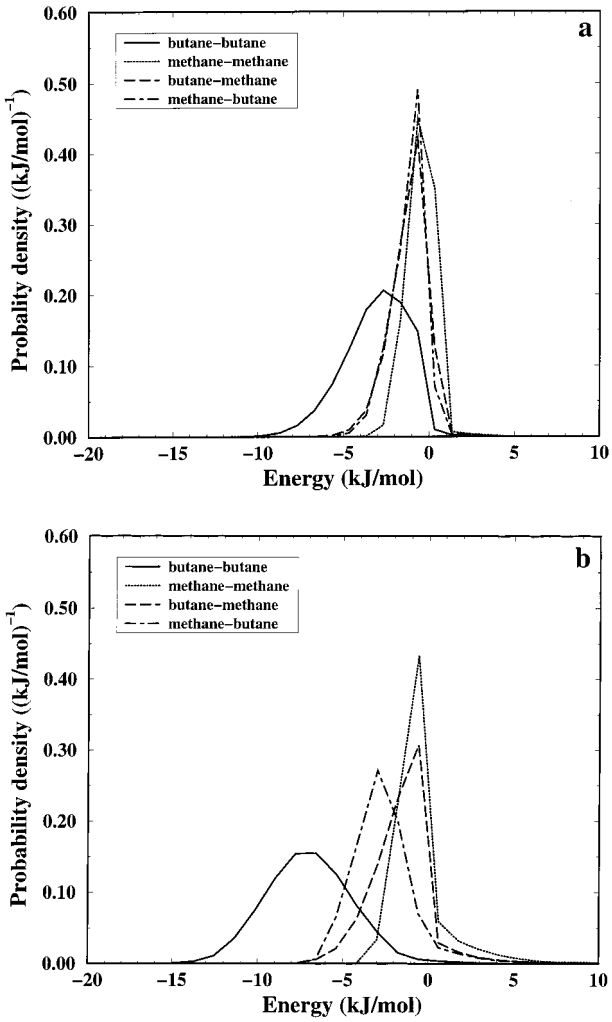

Figure 18. Distributions of sorbate−sorbate interaction energies experienced by each species residing in a straight channel at a loading of (a) 4 methane and 4 *n*-butane molecules/uc and (b) 4 methane and 9 *n*-butane molecules/uc. The designation "butane−methane" indicates energies felt by *n*-butane molecules located in a straight channel due to methane molecules located anywhere in the zeolite.

an obstacle to the diffusion of methanes and other *n*-butanes. The dependence of the methane self-diffusivity on *n*-butane occupancy is much stronger than that of the *n*-butane self-diffusivity on *n*-butane occupancy: As the *n*-butane loading rises from 2 to 9 molecules per unit cell, $D_s^{CH_4}$ falls by a factor of 60, while $D_s^{C_4H_{10}}$ falls by a factor of 30.

4.6. Energy Distributions. It is interesting to study the interaction energies felt by each sorbate species in each of the three different silicalite environments due to the surrounding crystal and due to neighboring molecules. First we have calculated the energy distributions by taking into account sorbate−sorbate and sorbate−zeolite interactions but not torsional and bending energies. Results are presented in Figure 17a,b. At a loading of 4 *n*-butane and 4 methane molecules/uc (Figure 17a), straight and sinusoidal channel energy distributions are centered at the values of −17 and −52 kJ/mol for methane and *n*-butane, respectively. The absolute values of those energies are close to, but higher than, the experimental sorption energies reported for these molecules at low occupancy.[31,41] *n*-Butane molecules exhibit somewhat more attractive energies in sinusoidal channels than in straight channels, while intersections are more repulsive (effective energy barriers). Methane energies at the same loading show similar distributions in straight and sinusoidal channels. When the loading is increased to 9 *n*-butane and 4 methane molecules per unit cell, the distributions shift to more attractive energy values, as expected (Figure 17b). It is interesting that sinusoidal channel energies are now almost the same as straight channel energies for *n*-butane. The changes in methane energy distributions are also interesting. Clearly, the change from 4 to 9 *n*-butane molecules/uc results in a broadening of the methane energy distribution in both channels and intersections, while the distribution in intersection interiors shifts to values of energy very close to those of the channel segments. Note that these differences between low- and high-occupancy systems are reflected in the populations of Figure 5; one should bear in mind, however, that the latter depend also on conformational energy and entropy effects.

Distributions of sorbate−sorbate interaction energies for molecules located in the straight channel regions are shown in Figure 18a,b. Figure 18a refers to a loading of 4 methane and 4 *n*-butane molecules/uc, while Figure 18b refers to a loading of 4 methane and 9 *n*-butane molecules/uc. From Figure 18a it is clear that *n*-butane−*n*-butane interactions are more attractive than methane−methane, *n*-butane−methane, and methane−*n*-butane interactions, because of the larger size of the *n*-butane molecules. *n*-Butane−methane and methane−*n*-butane distributions are almost the same. Increasing the loading brings about striking changes in the distributions (Figure 18b). *n*-Butane−

n-butane and methane−*n*-butane energy distributions clearly shift to more attractive values, as expected since we have increased the content of the mixture in *n*-butane. They become broader, indicating a wider multiplicity of relative configurations of the interacting molecules (especially for *n*-butane−*n*-butane interactions).

Methane−methane distributions, on the other hand, exhibit a small broadening toward more repulsive energies. Basically, *n*-butanes have their way, and methanes occupying the remaining space may be squeezed together (repulsive energies), probably in the case where they are sandwiched between two *n*-butane molecules.

Summary and Conclusions

Results from molecular dynamics simulations of binary mixtures of *n*-butane−methane in silicalite at various loadings and compositions have been reported. Equilibrium properties, such as siting of the sorbed species in different silicalite environments, have been seen to remain unchanged in the low-loading regime. Even for a fluid mixture consisting of 4 molecules per unit cell of each one of the two species, siting preferences retain their pure component characteristics: both species prefer to occupy the channel interiors, avoiding the energetically unfavorable intersection regions. In addition, the siting of methane preserves its delocalized character.

Interesting deviations, however, have been seen for the individual component behavior at higher loadings, particularly close to saturation. In the extreme loading of 14 methane and 4 butane molecules per unit cell, significant changes in the distributions were seen, with the two different species located primarily in different, well-defined, nonoverlapping regions inside the pore interiors. In particular the *n*-butane molecules were seen to prefer channel segments (both sinusoidal and straight), pushing the smaller methane molecules to the intersection regions. This fluid component separation was particularly prominent at a loading of 4 methane and 9 *n*-butane molecules per unit cell. Here, methane molecules were clearly forced by the *n*-butane molecules to abandon straight channel interiors, thus making space for the accommodation of the excess *n*-butane molecules. The above pictures were found to be consistent with center of mass pair distribution function studies.

The conformation of sorbed *n*-butane molecules was found to be strongly occupancy-dependent. A clear shift toward gauche conformations was seen at high loadings of both *n*-butane and methane; the resulting more compact shape of *n*-butanes allows more molecules to pack in the energetically more favorable channel regions.

By further study of the mean-square displacement of the center of mass along the three coordinate axes, a strong anomalous diffusion behavior was seen, particularly for the higher loadings. This anomalous diffusion has been documented to be due to correlated motion of the sorbed molecules, which is more pronounced for the smaller methane molecules, as the slowly moving *n*-butane molecules act as obstacles to their motion. The motion was seen to be particularly slow in the *z*-direction, where the crossover to Fickian diffusion regime even for methane was observed to occur at times on the order of nanoseconds.

Calculating the three components of the self-diffusivity tensor necessitated particularly long simulation times, sometimes on the order of 20 ns. Self-diffusivities have been calculated as functions of mixture loading and composition and have been seen to decrease monotonically with the concentration of either component. As an indication of the dramatic role played by the loading, we mention that the methane self-diffusivity was calculated to drop by a factor of 60 as the *n*-butane loading rises from 2 to 9 molecules per unit cell; the corresponding *n*-butane self-diffusivity was calculated to drop by a factor of 30.

The distributions of sorbate−sorbate and sorbate−zeolite interaction energies showed a clear occupancy dependence. By an increase of the loading from 4 methane and 4 *n*-butane to 4 methane and 9 *n*-butane molecules per unit cell, total (sorbate−zeolite and sorbate−sorbate) interaction energies in the three crystal environments shift to more attractive energies. *n*-Butane−*n*-butane and methane−*n*-butane energy distributions become broader and more attractive upon increasing the loading, while methane−methane energy distributions develop a repulsive tail, indicating squeezing together of methane pairs packed in available intracrystalline spaces.

Acknowledgment. We thank Dr. V. G. Mavrantzas, Dr. R. H. C. Jannsen, Dr. H. Jobic, and Prof. E. J. Maginn for helpful discussions. We also thank the Institute of Chemical Engineering and High Temperature Chemical Processes for generously providing part of the computer resources used in this work. We gratefully acknowledge the General Secretariat of Research and Technology of Greece for financial support in the form of a PENED'95 program, No. 218.

References and Notes

(1) Barrer, R. M. *Zeolites and Clay Minerals*; Academic Press: London, 1978.
(2) Kärger, J.; Ruthven, D. M. *Diffusion in Zeolites and Other Microporous Solids*; Wiley-Interscience: New York, 1992.
(3) Ruthven, D. M.; Farooq, S.; Knaebel, K. S. *Pressure Swing Adsorption*; WCH Publishers: New York, 1994.
(4) Chen, N. Y.; Degnan, T. F., Jr.; Smith, C. M. *Molecular Transport and Reaction in Zeolites*; Wiley-Interscience: New York, 1992.
(5) Woods, G. B.; Rowlinson, J. S. *J. Chem. Soc., Faraday Trans. 2* **1989**, *85*, 765.
(6) Woods, G. B.; Panagiotopoulos, A. Z.; Rowlinson, J. S. *Mol. Phys.* **1988**, *63*, 49.
(7) Razmus, D. M.; Hall, C. K. *AIChE J.* **1991**, *37*, 769.
(8) Karavias, F.; Myers, A. L. *Mol. Simul.* **1991**, *8*, 51.
(9) Maddox, M. W.; Rowlinson, J. S. *J. Chem. Soc., Faraday Trans.* **1993**, *89*, 3619.
(10) Van Tassel, P. R.; Davis, H. T.; McCormick, A. V. *Langmuir* **1994**, *10*, 1257.
(11) Van Tassel, P. R.; Davis, H. T.; McCormick, A. V. *Mol. Simul.* **1996**, *17*, 239.
(12) Buss, E.; Heuchel, M. *J. Chem. Soc., Faraday Trans.* **1997**, *93*, 1621.
(13) Heuchel, M.; Snurr, R. Q.; Buss, E. *Langmuir* **1997**, *13*, 6795.
(14) Snurr, R. Q.; Kärger, J. *J. Phys. Chem. B* **1997**, *101*, 6469.
(15) Funke, H. H.; Argo, A. M.; Baertsch, C. D.; Falconer, J. L.; Noble, R. D. *J. Chem. Soc., Faraday Trans.* **1996**, *92*, 2499.
(16) Funke, H. H.; Kovalchick, M. G.; Falconer, J. L.; Noble, R. D. *Ind. Eng. Chem. Res.* **1996**, *35*, 1575.
(17) Funke, H. H.; Argo, A. M.; Falconer, J. L.; Noble, R. D. *Ind. Eng. Chem. Res.* **1997**, *36*, 137.
(18) Chitra, R.; Yashonath, S. *Chem. Phys. Lett.* **1995**, *234*, 16.
(19) Jost, S.; Fritzsche, S.; Haberlandt, R. *Chem. Phys. Lett.* **1997**, *219*, 385.
(20) Jost, S.; Bar, N. K.; Fritzsche, S.; Haberlandt, R.; Kärger, J. *J. Phys. Chem. B* **1998**, *102*, 6375.
(21) Bandyopadhyay, S.; Yashonath, S. *J. Chem. Phys.* **1996**, *105*, 7223.
(22) Bandyopadhyay, S.; Yashonath, S. *J. Phys. Chem. B* **1997**, *101*, 5675.
(23) Olson, D. H.; Kokotailo, G. T.; Lawton, S. L.; Meier, W. M. *J. Phys. Chem.* **1981**, *85*, 2238.
(24) June, L. R.; Bell, A. T.; Theodorou, D. N. *J. Phys. Chem.* **1991**, *95*, 8866.
(25) Goodbody, S. J.; Watanabe, K.; MacGowan, D.; Walton, J. P.; Quirke, N. J. *J. Chem. Soc., Faraday Trans.* **1991**, *87*, 1951.
(26) Demontis, P.; Fois, E. S.; Suffritti, D. N. *J. Phys. Chem.* **1990**, *94*, 4329.
(27) Titiloye, J. O.; Parker, S. C.; Stone, F. S.; Catlow, C. R. A. *J. Phys. Chem.* **1991**, *95*, 4038.

(28) Santikary, P.; Yashonath, S. *J. Phys. Chem.* **1994**, *98*, 9252.
(29) June, L. R.; Bell, A. T.; Theodorou, D. N. *J. Phys. Chem.* **1992**, *96*, 1051.
(30) Maginn, E. J.; Bell, A. T.; Theodorou, D. N. *J. Phys. Chem.* **1993**, *97*, 4173.
(31) June, L. R.; Bell, A. T.; Theodorou, D. N. *J. Phys. Chem.* **1990**, *94*, 1508.
(32) Frenkel, D.; Smit, B. *Understanding Molecular Simulation: from algorithms to applications*; Academic Press: San Diego, CA, 1996.
(33) Edberg, R.; Evans, D. J.; Morriss, G. P. *J. Phys. Chem.* **1990**, *94*, 1508.
(34) Allen, M. P.; Tildesley, D. J. *Computer Simulation of Liquids*; Oxford University Press: Oxford, U.K., 1987.
(35) Chitra, R.; Yashonath, S. *J. Phys. Chem. B* **1997**, *101*, 5437.
(36) Maginn, E. J.; Bell, A. T.; Theodorou, D. N. *J. Phys. Chem.* **1995**, *99*, 2057.
(37) Snurr, R. Q.; Bell, A. T.; Theodorou, D. N. *Mol. Simul.* **1991**, *8*, 73.
(38) Bell, A. T.; Maginn, E. J.; Theodorou, D. N. In *Handbook of Heterogeneous Catalysis;* Ertl, G., Knözinger, H., Weitkamp, J., Eds.; VCH: Weinheim, Germany, **1997**; Vol. 3, p 1165.
(39) Hahn, K.; Kärger, J.; Kukla V. *Phys. Rev. Lett.* **1996**, *76*, 2762.
(40) Chassapis, C. S.; Petrou, J. K.; Petropoulos, J. H.; Theodorou, D. N. *Macromolecules* **1996**, *29*, 3615.
(41) Chiang, A. S.; Dixon, A. G.; Ma, Y. H. *Chem. Eng. Sci.* **1984**, *39*, 1451.